Hierarchical Micro- and Mesoporous Carbide-Derived Carbon as a High-Performance Electrode Material in Supercapacitors

*Marcus Rose, Yair Korenblit, Emanuel Kockrick, Lars Borchardt, Martin Oschatz, Stefan Kaskel, and Gleb Yushin**

Ordered mesoporous carbide-derived carbon (OM-CDC) materials produced by nanocasting of ordered mesoporous silica templates are characterized by a bimodal pore size distribution with a high ratio of micropores. The micropores result in outstanding adsorption capacities and the well-defined mesopores facilitate enhanced kinetics in adsorption processes. Here, for the first time, a systematic study is presented, in which the effects of synthesis temperature on the electrochemical performance of these materials in supercapacitors based on a 1 M aqueous solution of sulfuric acid and 1-ethyl-3-methylimidazolium tetrafluoroborate ionic liquid are reported. Cyclic voltammetry shows the specific capacitance of the OM-CDC materials exceeds 200 F g^{-1} in the aqueous electrolyte and 185 F g^{-1} in the ionic liquid, when measured in a symmetric configuration in voltage ranges of up to 0.6 and 2 V, respectively. The ordered mesoporous channels in the produced OM-CDC materials serve as ion-highways and allow for very fast ionic transport into the bulk of the OM-CDC particles. At room temperature the enhanced ion transport leads to 75% and 90% of the capacitance retention at current densities in excess of ~10 A g^{-1} in ionic liquid and aqueous electrolytes, respectively. The supercapacitors based on 250–300 μm OM-CDC electrodes demonstrate an operating frequency of up to 7 Hz in aqueous electrolyte. The combination of high specific capacitance and outstanding rate capabilities of the OM-CDC materials is unmatched by state-of-the art activated carbons and strictly microporous CDC materials.

M. Rose, Y. Korenblit, Prof. G. Yushin
School of Materials Science and Engineering
Georgia Institute of Technology
Atlanta, GA 30332, USA
E-mail: yushin@gatech.edu
M. Rose, L. Borchardt, M. Oschatz, Prof. S. Kaskel
Department of Inorganic Chemistry
Dresden University of Technology
D-01069 Dresden, Germany
Dr. E. Kockrick
Institut de Recherche sur la Catalyse et l'Environnement de Lyon
Universite Lyon 1
F-69626 Villeurbanne Cedex, France

DOI: 10.1002/smll.201001898

1. Introduction

Due to factors such as population growth and increasing energy and power demands around the globe, one of the key challenges facing scientists is the development of efficient electrical energy storage devices with application-tuned characteristics to guarantee the availability of on-demand energy and power. Electrochemical double-layer capacitors (EDLCs) or supercapacitors are considered to hold the most promise for mobile high-power energy storage technology with ultralong cycle life.[1] The main operating principle of these devices is based on the electrostatic adsorption of electrolyte ions on the large inner surface of porous electrodes. In spite of the higher capacitance offered by conductive polymers,[2] the great cycle stability and high electrical

small NANO MICRO

conductivity of porous carbon make it the material of choice for commercial EDLC electrodes. These electrodes are made of electrically conductive activated carbons (ACs) with a specific surface area in excess of 1500 m^2 g^{-1}. Natural precursor materials, such as coconut shells, make up the largest fraction of the market. The ACs used in most EDLCs exhibit a specific capacitance in the range of 80–110 F g^{-1} (40–70 F cm^{-3}) in organic electrolytes and ionic liquids and 100–160 F g^{-1} (50–80 F cm^{-3}) in aqueous electrolytes. The characteristic charge–discharge time of commercial EDLCs is in the range of 5–30 s. Highly desired improvements in the power storage capabilities of EDLCs require shorter characteristic charging–discharging time τ of these devices combined with higher specific capacitance C and/or larger cell voltage V (cell energy: $E \approx 0.5CV^2$; cell power $P \approx E/\tau$). Electrolytes used in EDLCs may be divided into three classes: aqueous (commonly stable to 0.6–1 V in EDLC); organic (commonly stable to 2.2–2.6 V in EDLC); and ionic liquids (ILs; commonly stable to 2.6–4.0 V in EDLC). The advantages of using aqueous electrolytes include their low cost and higher ionic conductivity. The advantages of ILs include high voltage stability (and thus high energy density) and lack of flammability, while their key disadvantage is a relatively low ionic mobility at and below room temperature, which results in slow charge/discharge. The characteristics of organic electrolytes lie somehere in between aqueous and ILs in terms of price, voltage, and charge–discharge time. Yet, their flammability creates concerns in many important mobile applications, including hybrid electrical vehicles (HEVs).

Traditionally, a Helmholtz electrical double layer (EDL) consisting of solvated ions was used to understand the energy storage mechanism. However, recent studies suggested substantial enhancement of capacitance for pores smaller than the size of solvated ions.[3] Inside these small micropores the solvation shell of the ions becomes highly distorted and partially removed, and the resulting smaller charge separation distance between the ion centers and pore walls leads to greatly increased capacitance.[3] In this case ions do not create layers on the surface of both walls of the slit-shaped pores nor coat the inner surface of the cylinder-shaped pores. Instead, more appropriate models of ion electrosorption would constitute formation of an ion monolayer sandwiched between slit pore walls or formation of an ion wire inside a cylindrical pore.[3b,4] Yet, when the pore size becomes too small, the access of the ions into the pores becomes limited and the kinetics of the ion transport are adversely impacted.[3c,5] Slightly larger well-aligned pores are needed for rapid charging/discharging.[6] Interestingly, experiments with IL with no solvent molecules revealed higher specific capacitance in small pores.[7] Therefore, a tight control over the carbon pore size distribution in the micropore range (primarily in the 0.5–1 nm range) is critically important for maximizing the energy storage characteristics of EDLCs, while the co-existence of straight pores connecting the particles' surface and their core (primarily in the range of 1–3 nm) is needed for improvements in the power characteristics of EDLCs.

The use of carbide precursors for porous carbon (carbide-derived carbon, CDC) formation is an attractive route to control the particle size, morphology, and structure[8] while allowing for the manipulation of the micropore (<2 nm) size distribution in carbons.[3c,9] CDC particles are commonly produced by high-temperature chlorination of metal carbides.[3c,9] Control over the synthesis conditions and the carbide selection allows for a narrow pore size distribution in CDC with a sub-Å precision with an average pore size in the range of 0.6–1.6 nm and the ability to attain a specific surface area of up to 2800 m^2 g^{-1}.[9a,10] Such properties allowed CDC to demonstrate outstanding capacitance characteristics in supercapacitors based on aqueous,[5] organic,[3c,9c,11] and IL electrolytes.[7,12] Yet, the narrow pores in CDC significantly suppress the ion motion within individual particles. Decreasing the particle size to sub-micrometer dimensions increased the rate capability only moderately.[11c] Using a novel approach this limitation can be overcome by designing CDC particles additionally having straight ordered mesopores, as we demonstrated in our recent study.[13] According to our method, the mesopore system of the SBA-15 silica template is infiltrated with a polymeric carbide precursor, such as polycarbosilane. The infiltrated template is then pyrolyzed under inert atmosphere, which leads to the formation of the metal carbide. After synthesis, the silica template matrix is washed away using hydrofluoric acid or sodium hydroxide. Subsequently, the "negative" replica structure with the inverse mesopores (former pore walls) is treated at a high temperature under a chlorine atmosphere to remove the metal atoms, resulting in highly microporous pore walls. In our first electrochemical experiments using organic electrolytes, these hierarchical ordered micro- and mesoporous CDC (OM-CDC) materials demonstrated significantly better power and energy storage characteristics than templated activated carbons produced using similar SBA-15 templates and organic precursors.[14] In addtion to their high specific surface area and high specific capacitance, the OM-CDCs showed significantly improved transport kinetics. The key advantage of the novel OM-CDC system is the very precise and independent control of the pore size in the micropore (0.5–2 nm) and mesopore (>2 nm) ranges.

Here we present the results of further systematic studies on these materials for application as electrode material in EDLCs. Specifically, we have investigated the influence of the chlorination temperature and the ordering in SiC-derived mesoporous carbons on the specific capacitance in 1 M aqueous solution of sulfuric acid (H_2SO_4) and in 1-ethyl-3-methylimidazolium tetrafluoroborate ($EMIBF_4$), a promising room temperature ionic liquid having relatively high ionic conductivity (15.7 mS cm^{-1}) and low viscosity (36.2 cP) at room temperature.[12,15]

2. Results and Discussion

2.1. Structure and Porosity

OM-CDC has been synthesized via formation and chlorination of mesoporous SiC.[13] Selective etching of Si from the SiC leads to the formation of uniform pores within the resultant CDC.[3c,9] Due to the porous nature of the SiC precursor, OM-CDC could be prepared at a temperature

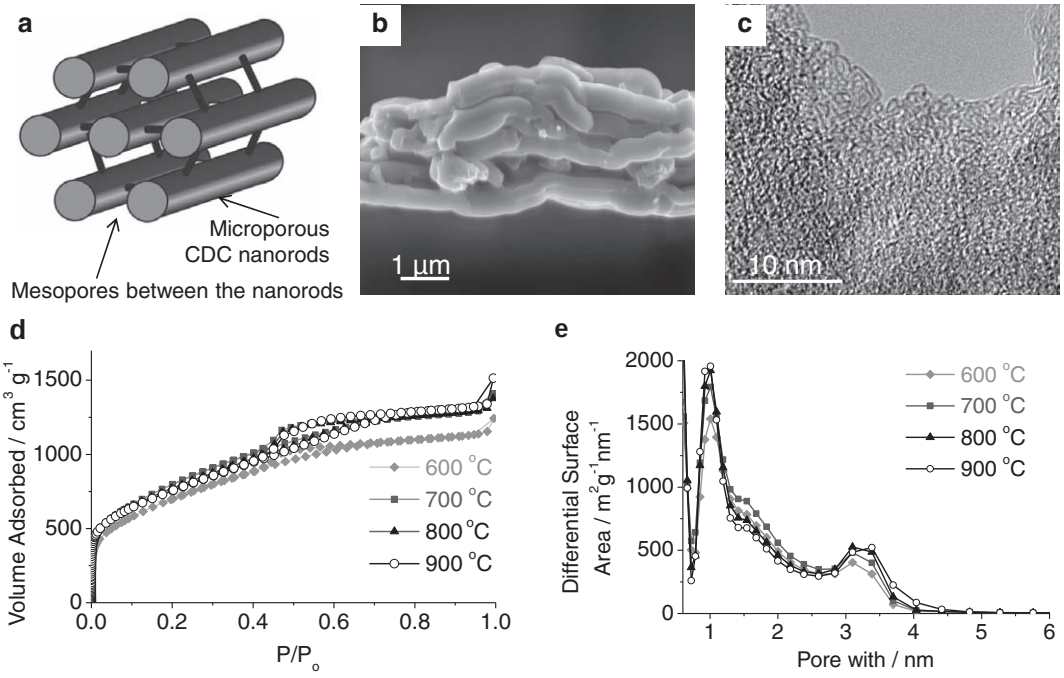

Figure 1. Structure and porosity of OM-CDC materials synthesized at different temperatures: a) schematic microstructure; b) scanning electron microscopy (SEM) and c) TEM images showing typical particle morphology and microstructure; d) N_2 gas sorption isotherms; and e) quenched solid density functional theory (QS-DFT) pore size distribution.

as low as 600 °C, which is 300 °C lower than the minimum chlorination temperature needed for the complete transformation of nonporous SiC micropowder into CDC.[9a,11c] In addition to micropores of ~1 nm commonly formed in SiC CDC,[8,11c] the conformal nature of the transformation[8] also allowed for the retention of the straight mesopores existing in the SiC precursor powder, leading to a dual pore-size distribution in the OM-CDC (**Figure 1**a). The produced CDC particles exhibit an elongated shape, commonly 10–20 µm in length and 2–5 µm in diameter (Figure 1b). Each particle is an agglomerate of smaller primary particles of comparable length but smaller diameter. Each primary particle consists of interconnected microporous CDC nanorods spaced at a regular distance from each other (Figure 1a). High-resolution transmission electron microscopy (TEM) revealed a highly disordered porous carbon structure (Figure 1c), very similar to that previously observed in SiC CDC.[8,9b] The purity of the OM-CDC samples was rather high, particularly those synthesized at 900 °C (**Table 1**). The residues detected included traces of Si, Cl, and Ca. The OM-CDC produced at 700 °C contained the highest content of chlorine residues, while the sample produced at 900 °C did not contain any detectable amount of impurities at all (Table 1).

The N_2 sorption isotherms collected at –196 °C on all of the mesoporous CDC samples are very similar and are typical for porous materials having both micro- and mesopores (Figure 1d). They show high N_2 adsorption at low relative pressure (P/P_0) due to the presence of micropores and additionally uptake at P/P_0 = 0.2–0.8 due to the high mesopore content. The formation and disappearance of hysteresis loops (due to the effect of capillary condensation) at the same P/P_0 for all the samples (Figure 1d) suggests that the samples have very similar mesopore sizes. The pore volume for all but the 600 °C sample (determined at P/P_0 = 0.95) is nearly identical (**Table 2**).The specific surface areas of the samples are exceptionally high (up to 2729 m^2 g^{-1}, Table 2), due to the combination of a large external surface area of CDC

Table 1. Impurities remaining in the OM-CDC materials.

Sample	Cl	Si	Ca
mesoporous CDC, 600 °C	1.2%	0.4%	1.2%
mesoporous CDC, 700 °C	3.5%	0.4%	0.3%
mesoporous CDC, 800 °C	1.3%	0.2%	0.2%
mesoporous CDC, 900 °C	<0.1%	<0.1%	<0.1%

Table 2. Porosity properties of the OM-CDC materials.

Sample	SSA[a)] [m^2 g^{-1}]	MPV[b)] [cm^3 g^{-1}]	TPV[c)] [cm^3 g^{-1}]
mesoporous CDC, 600 °C	2364	1.00	1.60
mesoporous CDC, 700 °C	2708	1.14	1.84
mesoporous CDC, 800 °C	2729	1.16	1.92
mesoporous CDC, 900 °C	2669	1.14	2.00

[a)]Brunauer–Emmett–Teller (BET) specific surface area measured for P/P_0 = 0.05–0.2; [b)]Micropore volume measured at P/P_0 = 0.2; [c)]Total pore volume measured at P/P_0 = 0.95.

NANO MICRO small

nanorods (Figure 1a)[13] and the well-developed microporosity within the CDC nanorods.

Unfortunately, such hierarchical pore systems with different pore sizes and shapes are difficult to characterize. Different methods have to be used to describe the pore filling mechanism in micropores and the capillary condensation in mesopores. Classical macroscopic methods such as Horvath–Kawazoe (HK), Saito–Foley (SF), or Dubinin–Radushkevich (DR) are mainly used for microporous materials, while the Barrett–Joyner–Halenda (BJH) and Dollimore–Heal (DH) methods are better suited for mesoporous materials since they are based on the Kelvin equation and take the capillary condensation into account. The macroscopic methods based on statistical mechanics using density functional theory (DFT) are capable of analyzing adsorption in materials with a broad pore-size distribution. However, they commonly require well-defined and uniform pore shape. So far, DFT methods have been developed for slit-shaped and cylindrical (cyl.) pores. The shape of the micropores in CDC can be best described using a slit-pore model.[3c,9b] However, the pores between the CDC nanorodes have an "inverse cylindrical" shape, and the existing DFT models might only qualitatively describe their mesopore size. In order to describe the N_2 adsorption in small mesopores (<6–7 nm), one has to consider both the interaction of the adsorbate with the pore walls and the capillary condensation effects.[16] The strength H of the interaction of fluids with pore walls decreases in the following order of pore shapes: $H_{cyl.} > H_{slit} > H_{inverse\ cyl.}$. The sum of all the interactions between the N_2 adsorbate and the pore surface atoms in inverse cylindrical pores (pores between the CDC nanorods, Figure 1a) is weaker than that in slit-shaped pores of the same size because these interactions rapidly diminish with separation distance. Therefore, if the capillary condensation effects could be completely ignored, the slit-shaped-pore DFT model would overestimate the size of the mesopores. On the other hand, if one considers only the capillary condensation and ignores the fluid-pore wall interactions, then the slit-shaped model would slightly underestimate the size of the mesopores because the average curvature of the N_2 fluid meniscus is slightly higher in the case of inverse cylindrical pores (the meniscus in slit-shaped pores is not curved in the direction parallel to the pore walls). Therefore, in our case these two effects should partially counter-balance each other and reasonable estimation of the mesopore size could be obtained using a slit-pore model (Figure 1e). In contrast, the cylindrical pore shape model would significantly overestimate our mesopore size.

Among the DFT models available, we have selected a quenched solid DFT (QS-DFT) model (Figure 1e) which has been specifically developed for disordered micro/mesoporous carbons with heterogeneous surface chemistry. This model gave us a threefold decrease in the fitting error as compared to the previously utilized nonlinear DFT model.[14] The drop in the pore size distribution at around 0.7 nm is an artifact of the DFT model. As expected from the isotherms (Figure 1d), the pore size distribution in OM-CDC samples was very similar. It contained a peak at ~1 nm, as in conventional microporous SiC-CDC powder samples,[9b,11c] and an additional broader peak at ~3 nm. No pores above 4 nm could be detected. The samples produced by chlorination at higher temperatures showed marginally larger mesopores (Figure 1e).

Besides porosity, another important factor for EDLC materials is the carbon microstructure. As shown previously, a higher chlorination temperature commonly leads to a higher graphitization degree.[9a,9b,11c] This effect can be qualitatively characterized by measuring the Raman spectra (Figure 2a) and comparing the integrated intensities of the D-band originating from disordered carbon at ~1340 cm^{-1} and the G-band from graphitic carbon at ~1590 cm^{-1}.[17] The samples chlorinated at temperatures between 600 and 900 °C reveal a small but consistent decrease of the ratio of the D- and G-bands' intensities, I_D/I_G (**Figure 2**b), supporting previous measurements.[9a,9b,11c] The lower I_D/I_G ratio is commonly associated with an ordering and the decrease in the concentration of defects. Interestingly, we observed a noticeable difference between the Raman spectra of the samples used in this study and the Raman spectra of similarly produced samples described in our previous publication.[14] Specifically, the I_D/I_G ratio in our new samples was lower. Presumably, the lower degree of disorder observed in the new samples could be linked to the replacement of the previously utilized postchlorination treatment in ammonia at 600 °C[14] with a similar treatment in hydrogen at identical conditions.

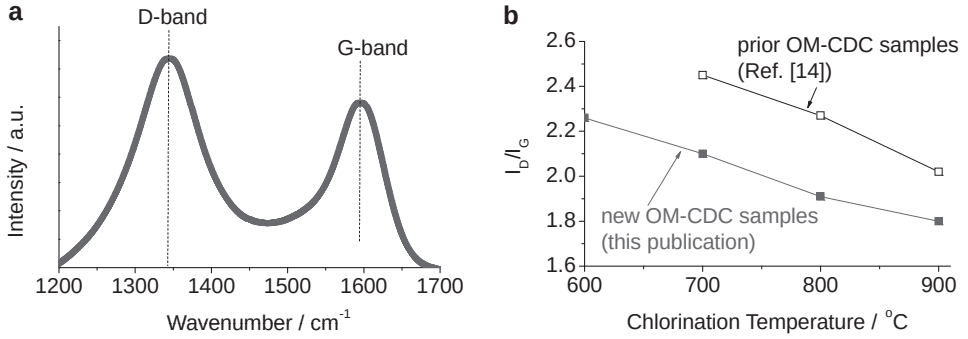

Figure 2. Raman spectroscopy studies of OM-CDC: a) a typical Raman spectra of the OM-CDC sample synthesized at 900 °C; b) I_D/I_G ratio as a function of synthesis temperature.

Reactive atomic hydrogen species produced upon ammonia decomposition at elevated temperatures could have induced additional defects in CDC.[14] A potentially lower content of amorphous carbon in the new samples correlates well with the observation of increased specific surface areas (compare Table 1 and reference [14]).

2.2. Electrochemical Performance

2.2.1. Ionic Liquid Electrolyte: $EMIBF_4$

The use of ILs as electrolytes for supercapacitors is an emerging but a very important research area in the field due to the exceptionally good thermal stabilities of ILs combined with their high maximum operating voltages and high conductivities at elevated temperatures.[12,18] Following the work of Kurig et al. on EDLCs based on TiC-CDC and IL,[12] we have selected 1-ethyl-3-methylimidazolium tetrafluoroborate ($EMIBF_4$) as a model room-temperature IL electrolyte to probe the performance of OM-CDC.

Cyclic voltammetry (CV) measurements revealed pseudocapacitance peaks visible at ~1 and ~1.7 V in the symmetrical EDLC (**Figure 3**a), which may result either from impurities present in the IL or from the reaction of the IL with the functional groups on the CDC surface. In spite of the redox reactions present, all the assembled devices demonstrated excellent stability. In fact, after 10 000 charge–discharge galvanostatic cycles between 0 and 2 V, the specific capacitances of the OM-CDC electrodes commonly retained 99–100% of the original values, indicating a high cycle stability of the employed CDC–$EMIBF_4$ electrochemical system. All the samples demonstrated very high specific capacitance values, reaching 175–186 F g^{-1} as measured by CV at 1 mV s^{-1}. These values significantly exceed that of high-performance activated carbons (such as YP-17D) or conventional microporous CDC when measured in the same voltage range (up to 2 V). As an important feature for high-power applications, the capacitance was largely retained when the sweep rate was increased from 1 to 100 mV s^{-1}. Interestingly, at the fastest sweep rate of 100 mV s^{-1} the redox reaction peaks are fully suppressed (Figure 3a), but the CV curve exhibited a nearly rectangular shape, which is characteristic of an ideal EDLC with little electrolyte diffusion limitations. Figure 3b further emphasizes the high room-temperature rate performance of EDLCs based on OM-CDC and ILs. OM-CDC samples retained up to 70% of the maximum specific capacitance when the sweep rate was increased from 1 to 100 mV s^{-1} (Figure 3b). In contrast, a high-rate commercial activated carbon YP-17D, developed and optimized for EDLC applications, retains only ~40% of the capacitance at 100 mV s^{-1}.

The maximum specific capacitance of the OM-CDC samples showed little dependence on the chlorination temperature, with OM-CDC synthesized at 600 °C and having the lowest surface area exhibiting the smallest capacitance (Figure 3b). The very small sample-to-sample variations in the specific capacitance recorded at different sweep rates could be explained by their very similar pore size distribution (Figure 1c).[7] In contrast to TiC, ZrC, Al_4C_3, Ti_3AlC_2, Ti_2AlC, Ti_3SiC_2, $Ti_2AlC_{0.5}N_{0.5}$, Ta_2AlC, Ta_2C, TaC, B_4C and many other carbides, the chlorination of SiC at different temperatures does not change the CDC micropore size significantly.[5,9b,10,19] Furthermore, the microstructure of SiC CDC produced at different temperatures remains largely amorphous with no formation of multiwalled graphene ribbons at chlorination temperatures of up to 1200 °C[8,9b] and rather moderate changes in the Raman spectra (Figure 2). Normalizing the capacitance by the internal surface area (Figure 3c) allowed us to detect only a marginal decrease in

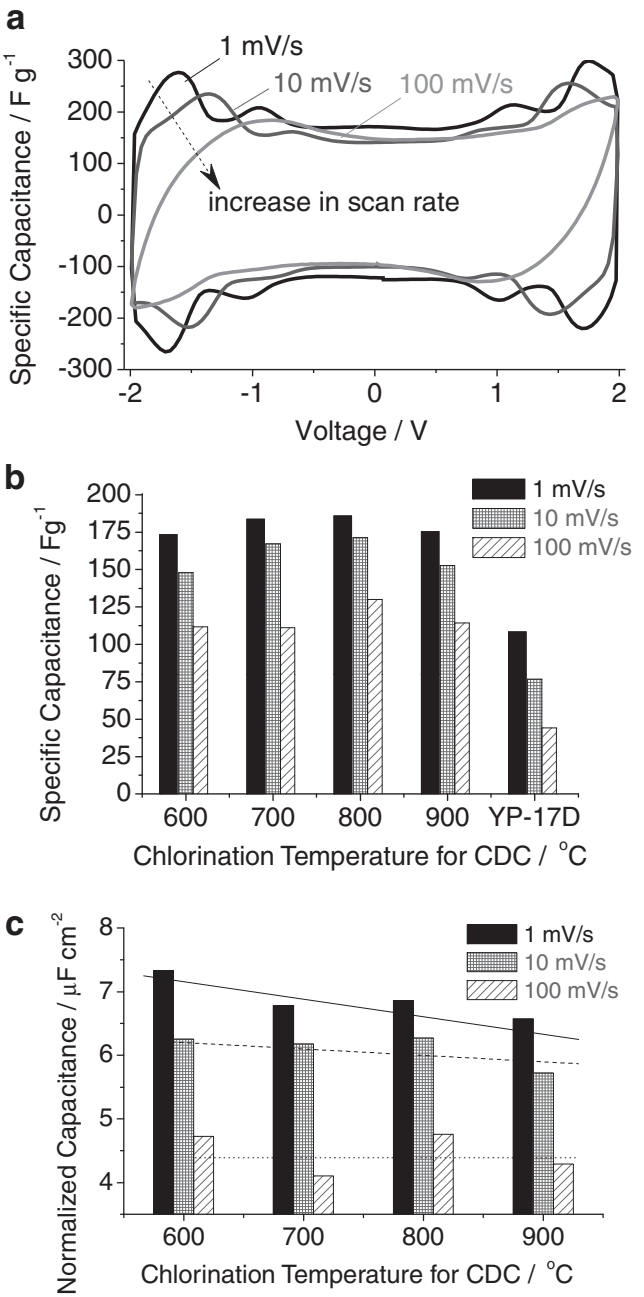

Figure 3. Electrochemical characterization of OM-CDC materials in $EMIBF_4$ ionic liquid at room temperature (20 °C): a) cyclic voltammogram of CDC synthesized at 900 °C; b) specific capacitance of CDC samples at different CV cycling rates in comparison with that of YP-17D activated carbon; c) BET area-normalized specific capacitance as a function of synthesis temperature.

small NANO MICRO

the maximum capacitance per unit area with increasing chlorination temperature. Similar data recorded at higher rates of 10 and 100 mV s^{-1} show no obvious trends.

To obtain insights into the effect of the OM-CDC synthesis temperature on the resistance and frequency response of EDLCs, we have performed impedance spectroscopy studies (**Figure 4**). The impedance spectra of EDLCs can be simulated by a transmission line equivalent circuit.[20] The simulated Nyquist plot (imaginary versus real component of the complex impedance) will contain two segments–the 45° segment at high frequency and the nearly vertical line at low frequency.[20] The length of the 45° segment (Figure 4a) is related to the resistance faced by the ions during their transport into the core of the OM-CDC particles. While the samples produced at 700–900 °C showed similar level of ionic resistance, the OM-CDC produced at the lowest temperature (600 °C) demonstrated a noticeably better performance. Since the size of the mesopores was, in fact, marginally smaller in the 600 °C sample (Figure 1d), we propose that higher synthesis temperatures caused some partial blockage of the mesopores, undetected by the gas sorption experiments. Similarly, in our prior studies of OM-CDC using organic electrolytes, the lowest synthesis temperature also led to the lowest ionic resistance.[14] The slightly lower specific capacitance of the OM-CDC produced at 600 °C could be linked to its lower surface area (Table 2) and the presence of Ca impurities (Table 1) which might have made smaller micropores inaccessible by the relatively large IL ions even at 1 mHz.

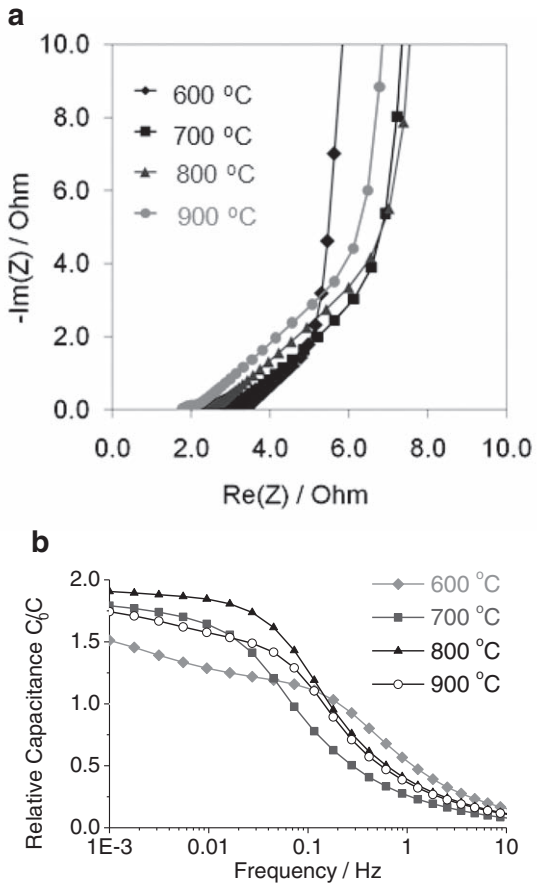

Figure 4. Electrochemical characterization of OM-CDC materials synthesized at different temperatures in $EMIBF_4$ ionic liquid at room temperature (20 °C): a) Nyquist plot, b) frequency response. C_0 in (b) is the specific capacitance of YP-17D measured at 0.001 Hz.

An equivalent series resistance (ESR) is another important characteristic of an EDLC cell. It is measured at high frequency where the imaginary component of the complex impedance becomes zero. The contributions to ESR include the electrical resistance of the electrodes and the electrode-current collector interfaces as well as the portion of the ionic resistance related to the ion transport outside of the carbon pore channels. Figure 4a shows a graduated decrease of the ESR with increase in the CDC synthesis temperature. Since the discussed portion of the ionic resistance is the same for all the samples, these results agree with previous observations of higher electrical conductivity of CDC produced at higher temperatures.[3c,5] The power performance of supercapacitors is influenced by the total internal resistance (TIR), which includes ESR and the resistance faced by ions moving within the electrode nanopores at a frequency, where electrolyte access has been made to most of the available surface area. The TIR, measured by the intersection of the projection of the near-vertical line to the real impedance axis in a Nyquist plot, is the lowest for the OM-CDC produced at 600 °C.

Figure 4b shows the frequency response of the EDLCs. The maximum frequency at which the capacitance decreases by no more than 50%, f_{max}, ranges from 0.1 to 0.7 Hz for the produced EDLCs. These are very high values for EDLCs with an IL electrolyte operating at room temperature. In fact, the measured f_{max} is even higher than that of commercial activated carbon-based EDLCs with organic electrolytes.[14] The straight mesopore channels (Figure 1a) in OM-CDCs are the likely cause for this enhanced performance. The best frequency response was observed in OM-CDC synthesized at 600 °C and having the lowest TIR, as expected from Figure 4a. The slow frequency response of the OM-CDC synthesized at 700 °C is likely related to the interaction of the IL electrolyte with chlorine residues detected in this sample (Table 1).

One of the key advantages of the OM-CDC materials in practical applications is their outstanding capacitance retention at high current densities (**Figure 5**). While the room-temperature capacitance of the YP-17D activated carbon in $EMIBF_4$ decreases to less than 25% of the maximum value when the current density increases to above 3 A g^{-1}, the OM-CDC samples are capable of retaining 75% of the capacitance at current densities in excess of 10 A g^{-1} (Figure 5). The significant decrease in the capacitance at high current density for the OM-CDC synthesized at 700 °C, likely originating from the chlorine residues remaining in this sample (Table 1), suggests the importance of an efficient purification procedure for the optimum OM-CDC performance in IL-based supercapacitors.

2.2.2. Aqueous Electrolyte: 1 M H_2SO_4

Excellent capacitance values, rapid transport, and electroadsorption of ions were also observed in aqueous electrolytes. CV experiments showed the absence of Faradaic charge transfer peaks (**Figure 6**a). This observation suggests that in contrast to other high-capacitance porous carbons,[6] OM-CDC samples treated with H_2 have a very low

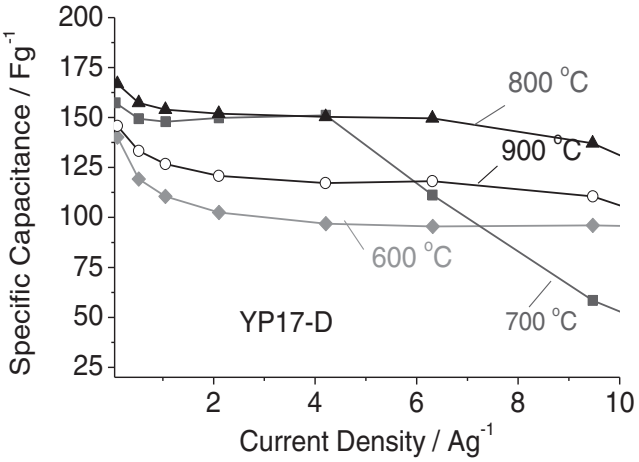

Figure 5. Electrochemical characterization of OM-CDC materials synthesized at different temperatures and YP17D in $EMIBF_4$ ionic liquid at room temperature (20 °C): capacitance retention with current density.

concentration of functional groups that contribute to redox reactions. The rectangular shape of the CV curves maintained at sweep rates as high as 500 mV s^{-1} (Figure 6a) indicates very fast ion transport within the OM-CDC, unachievable in conventional CDC powders[5,21] and activated carbons, including those that contain a high volume of large mesopores.[22]

In contrast to the performance of OM-CDC in ILs (Figure 3b,c), we observed that the chlorination temperature has a significant impact on the specific capacitance (Figure 6b). The highest value (202 F g^{-1}) was achieved in OM-CDC synthesized at the lowest temperature of 600 °C, in spite of its lowest BET specific surface area (Table 2). We note, however, that H_2SO_4 electrolyte solution has likely dissolved Ca impurities, which could have opened some of the smaller micropores. In addition, we cannot rule out a possible insertion/intercalation of the small ions into the pores not accessible by N_2 during gas sorption measurements (Table 2).

Conventional CDC particles at this relatively low temperature commonly contain a significantly higher amount of residues, which is difficult to remove using post-treatments in NH_4 or H_2. The remaining impurities clog the narrow micropores in CDC and commonly do not allow the specific capacitance in aqueous electrolytes to exceed 80–110 F g^{-1}.[5,21] Furthermore, conventional CDC powder synthesized at 600 °C exhibits a very rapid capacitance decrease when the sweep rate is raised above 20 mV s^{-1}.[5,21] In contrast, OM-CDC may retain up to 75% of the maximum capacitance when the sweep rate is increased to as high as 500 mV s^{-1}. The only other high-capacitance carbon that exhibit such properties in a thick (250–300 μm) electrode configuration is zeolite-templated carbon, which also has straight and well-aligned pore channels.[6] Even recently developed one-dimentional mesoporous carbon fibers with very high capacitance and large aligned mesopore channels between the individual fibers showed higher capacitance fading at increasing sweep rates.[23]

The influence of the OM-CDC synthesis temperature becomes even more evident when the capacitance is

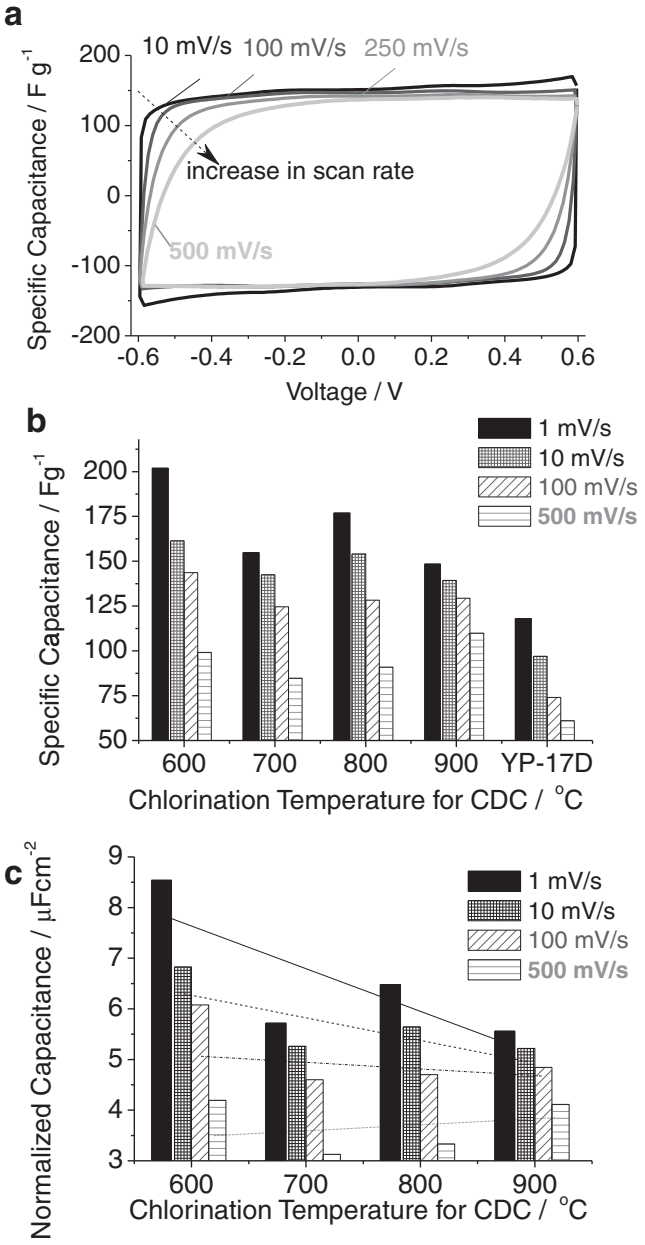

Figure 6. Electrochemical characterization of OM-CDC materials in 1 M H_2SO_4 at room temperature (20 °C): a) cyclic voltammogram of CDC synthesized at 900 °C; b) specific capacitance of CDC samples at different CV cycling rates in comparison with that of YP-17D activated carbon; c) BET area-normalized specific capacitance as a function of synthesis temperature.

normalized by the surface area (Figure 6c). Interestingly, the dependence practically disappears at faster scan rates (Figure 6c). We propose that the difference in the behavior of OM-CDC samples in aqueous versus IL electrolytes is primarily related to the interaction of the carbon defects (dangling bonds) with the solvation shells in aqueous electrolytes. Such interactions may reduce the electrolyte–carbon contact angle allowing the wetting of previously inaccessible pores[24] or assist in stripping the solvation shells when the ions enter the narrow micropores.[3c,5] A decrease in the specific capacitance in both strictly microporous[3c,5]

NANO MICRO small

and strictly mesoporous carbons[25] with a decrease in the concentration of surface defects has been consistently observed in various electrolyte solution systems.[3c,5,14,25] Therefore, the OM-CDC sample produced at 600 °C and containing the highest defect content (Figure 2b) exhibited the highest normalized capacitance. Yet, when the electrolyte does not contain solvent molecules, the effect of the carbon surface microstructure becomes significantly reduced (compare Figure 6b,c with Figure 3b,c).

Figure 7 shows the results of the impedance spectroscopy studies. Similarly to the results obtained with ILs (Figure 4a), higher chlorination temperature commonly leads to a decrease in the ESR (Figure 7a). In contrast to the performance of OM-CDC in ILs, however, the length of the 45° segment and thus the level of the ionic resistance is the highest for the 600 °C sample (Figure 7a). Such a result confirms the previous measurements (Figure 6) and likely originates from the interaction between surface defects and solvent molecules. The slower ion diffusion and the lower electrical conductivity in OM-CDC samples produced at lower temperatures led to the highest TIR for the 600 °C and the smallest for the 900 °C samples. The frequency response of OM-CDC/aqueous electrolyte-based EDLCs correlated well with the TIR trend and was exceptional (Figure 7b) with f_{max} ranging from 3 to 7 Hz. The small size and high mobility of ions in the aqueous electrolyte combined with the existence of ordered mesopores likely contributed to this excellent rate capability.

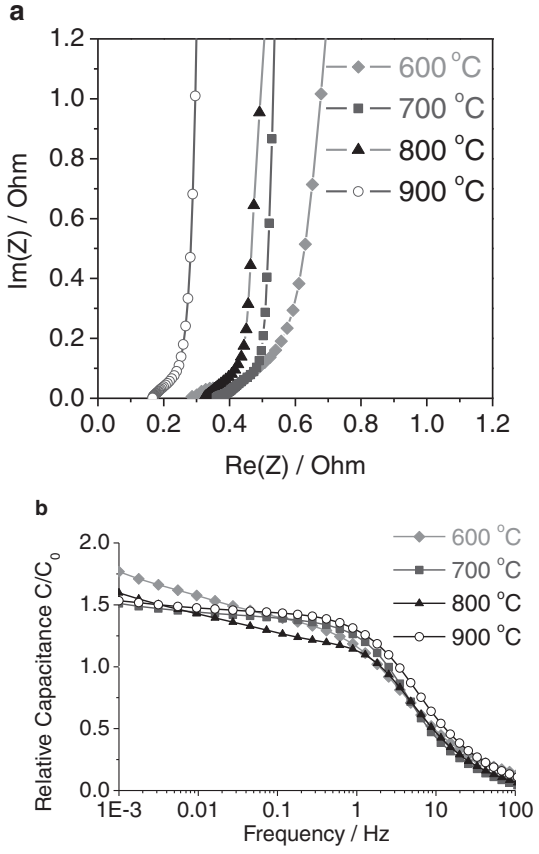

Figure 7. Electrochemical characterization of OM-CDC materials synthesized at different temperatures and YP17D in 1 M H_2SO_4 at room temperature (20 °C): a) Nyquist plot, b) frequency response. C_0 in (b) is the specific capacitance of YP-17D measured at 0.001 Hz.

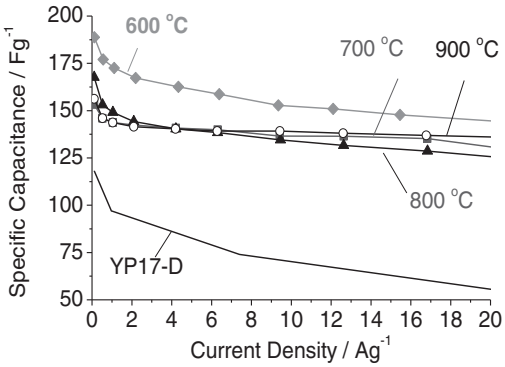

Figure 8. Electrochemical characterization of OM-CDC materials synthesized at different temperatures and YP17D in 1 M H_2SO_4 at room temperature (20 °C): capacitance retention with current density.

The capacitance retention at high current densities was also very good (**Figure 8**). The OM-CDC samples synthesized at higher temperature consistently showed a slightly better performance. The 900 °C sample, for example, retained nearly 90% capacitance when the current density was increased from 0.1 to over 20 A g^{-1} (Figure 8). In contrast, the high-rate activated carbon retains less than 50% at comparable current densities.

3. Conclusion

In summary, we have gained insight into the electrosorption properties and electrochemical performance of hierarchical micro- and mesoporous silicon carbide-derived carbons. OM-CDC samples synthesized at 600–900 °C demonstrated a specific surface area in the range of 2364 to 2729 m^2 g^{-1}, which is among the highest ever observed in CDC. The lowest surface area was demonstrated in OM-CDC synthesized at the lowest temperature of 600 °C. The chlorination temperature was not found to significantly affect the pore size distribution. In EDLCs based on either $EMIBF_4$ or 1 M H_2SO_4 electrolytes, OM-CDC samples synthesized at higher temperatures showed lower ESR. The chlorination temperature only moderately affected the specific capacitance and the overall electrochemical performance of OM-CDC in $EMIBF_4$, but had quite a significant effect on the electrochemical characteristics of OM-CDC in 1 M H_2SO_4 electrolyte solution. The interaction of solvent molecules with the carbon structural defects was proposed as a main explanation for the observed phenomena. Chlorine residues were found to affect the power characteristics of supercapacitors based on ionic liquids, but they did not have a significant effect on supercapacitors with a H_2SO_4 electrolyte. Due to the presence of straight mesopore channels combined with a high micropore content, the produced OM-CDC samples not only demonstrated very high specific capacitances of up to ~202 F g^{-1} in the aqueous electrolyte and ~186 F g^{-1} in the ionic liquid at room temperature, but also showed outstanding ion transport kinetics with the highest operating frequency reaching

~0.7 Hz and ~7 Hz in the ionic liquid and aqueous electrolyte, respectively. The best samples also demonstrated an exceptionally high power performance with up to 90% of the capacitance retained when the current density was increased from 0.1 to over 20 A g^{-1} in 1 M H_2SO_4 electrolyte solution. The combination of superb energy and power characteristics of the OM-CDC samples could not be matched by the state-of-the art activated carbons or microporous CDC. Further work will concentrate on the performance enhancement via the use of other metal carbide precursors, such as TiC and VC, with which significantly higher specific capacitances could be achieved. Additionally, other hierarchical structures for optimum ion transport kinetics are under investigation.

4. Experimental Section

Material Preparation: The mesoporous CDC materials were produced according to a synthesis route previous published by Krawiec et al.[13] High-quality ordered mesoporous SBA-15 was used as a template for the nanocasting process. It was infiltrated with a solution of polycarbosilane (PCS, Sigma-Aldrich) with an average molar weight of 800 g mol^{-1} in a mixture of *n*-heptane and *n*-butanol (20:1). The dried powder was pyrolyzed in a quartz boat at 1000 °C under a dynamic argon atmosphere in a tube furnace in order to convert the PCS in the pore system of the silica template to SiC. The resulting composite material was first treated with hydrofluoric acid in order to remove the silica template and subsequently washed at least three times with ethanol. The samples were chlorinated under a dynamic chlorine atmosphere for 3 h in a quartz boat in a tube furnace to convert the SiC into CDC. The chlorination temperature was varied between 600 and 900 °C. A subsequent treatment at 600 °C for 2 h under a hydrogen atmosphere was conducted to remove residual chlorides and chlorine.

Electrode Preparation: The electrodes for electrochemical characterization were produced as follows: Fine CDC powders (150 mg) were suspended in a small amount of ethanol mixed with 13.1 mg of a suspension of polytetrafluoroethylene (PTFE, 60 wt% in water, Sigma-Aldrich) binder. The resulting slurry of 95 wt% carbon and 5 wt% PTFE was concentrated by slow evaporation of the ethanol at 80 °C and moderate stirring. The highly viscous slurry was then slowly dried on a glass plate and mixed with a spatula until the mass became a rubberlike (clay) consistency. The resulting composite paste was predried in a vacuum oven at 80 °C for several hours and afterwards rolled to a thickness of ~250 μm using a commercial rolling mill. The electrodes for aqueous electrolyte were cut into squares of around 1 cm^2 while the electrodes for the ionic liquid assembled in a coin cell were punched out with a diameter of 0.5 inch (1 inch = 2.54 cm). The resulting electrodes were further dried at 80 °C in a vacuum oven for at least overnight before assembling the electrodes.

Device Assembly: The EDLCs were assembled in a symmetrical two-electrode configuration. Al foil of 300 μm in thickness was roughened using a 600 grit SiC sandpaper, coated by a thin layer (≈10–20 μm) of conductive paint (EB-012, Acheson Colloids, US) and used as a current collector for IL electrolytes. The conductive paint was used to reduce the interfacial resistance between the electrode and the current collector. An uncoated high-purity gold foil was used as a current collector for aqueous electrolyte EDLCs. A GORE membrane (W.L. Gore and Associates, US) of 25 μm in thickness and 60% porosity was used as a separator for the EDLC devices.

For IL-based EDLCs, the Al–electrode–separator–electrode–Al sandwich was assembled in a stainless steel coin cell configuration. The assembly was carried out in a glovebox (Innovative technologies, <1 ppm of H_2O). As electrolyte we selected 1-ethyl-3-methylimidazolium tetrafluoroborate (EMIBF$_4$, >98%, IoLiTec Ionic Liquids Technologies GmbH, Germany). A few droplets were used for wetting the electrodes and the separator during assembly. The excess amount was removed during compression of the coin cell. The coin cells were taken out of the glovebox, and small aluminum contacts were fixed with the above mentioned clamps.

For aqueous (1 M aqueous solution of H_2SO_4) EDLCs, the Au–electrode–separator–electrode–Au sandwich was assembled in a beaker-type cell configuration in open air. The sandwich was held together by Teflon slabs held together by Teflon screws. An excess amount of sulfuric acid was added to the beaker (~50 mL). The Au foil was shaped to both contain the electrodes in the sandwich and protrude out from the cell to allow for contact with the various characterization devices.

Characterization: The synthesized powders were characterized with regard to their porosity by nitrogen physisorption experiments at –196 °C using the Autosorb-1C from Quantachrome. Prior to the measurements the samples (ca. 50 mg) were degassed at 150 °C for at least 6 h under vacuum. The specific surface area (SSA) was determined according to the BET theory in the relative pressure range $P/P_0 = 0.05–0.2$. The micropore and total pore volume (MPV and TPV) were determined after Gurvich at a relative pressure of 0.2 and 0.95, respectively. The pore size distribution was investigated applying the QS-DFT equilibrium model for nitrogen on carbons with slit-shaped pores at –196 °C.

The degree of carbon ordering was investigated using micro-Raman spectroscopy. An Ar ion laser (488 nm) was used for excitation on a Ramascope 1000 Raman microspectrometer from Renishaw/UK equipped with a charged-coupled device (CCD) detector and an optical microscope for focusing the incident laser beam to a 1–2 μm spot size. The spectra were collected in the extended regime in the range of 800–1800 cm^{-1}. Prior to analysis, the microspectrometer was calibrated using a plain Si wafer. SEM was performed using a LEO 1530 scanning electron microscope (LEO, Osaka, Japan; now Nano Technology Systems Division of Carl Zeiss SMT, MA, USA). In-lens secondary electron detector was used for the studies, most of which were performed using an accelerating voltage of 5 kV and a working distance of 5 mm. TEM observations of CDC microstructure were carried out using a Philips CM200UT microscope (Philips, Netherlands) operated at an accelerating voltage of 200 kV.

The electrochemical testing of the synthesized materials included galvanostatic (constant current) charge–discharge measurements, electrochemical impedance spectroscopy (EIS) and cyclic voltammetry (CV). The EIS tests were carried out using a Zahner IM6 electrochemical workstation (Zahner-Elektrik GmbH & CoKG, Kronach, Germany) in the frequency range of 1 mHz to 100 kHz with a 10 mV AC amplitude. CV measurements were carried out using the same device with sweep rates of 100, 10, and 1 mV/s in the voltage range of –2 to +2 V and –0.6 to +0.6 V in IL

small NANO MICRO

and aqueous electrolytes, respectively. The charge–discharge tests were carried out using an Arbin SCTS supercapacitor testing system (Arbin Instruments, TN, US) between 0 to +2 V at charge/discharge current densities between 100 and 20 000 mA g^{-1}, based on the mass of a single electrode.

Acknowledgements

This work was partially supported by Nanomat (contract # DFG-SPP 1181) and AFOSR (grant # FA9550-09-1-0176).

[1] P. Simon, Y. Gogotsi, *Nat. Mater.* **2008**, *7*, 845.

[2] I. Kovalenko, D. Bucknall, G. Yushin, *Adv. Funct. Mater.* **2010**, *20*, 3979.

[3] a) G. Feng, R. Qiao, J. S. Huang, B. G. Sumpter, V. Meunier, *ACS Nano* **2010**, *4*, 2382; b) J. S. Huang, B. G. Sumpter, V. Meunier, *Angew. Chem. Int. Ed.* **2008**, *47*, 520; c) J. Chmiola, G. Yushin, Y. Gogotsi, C. Portet, P. Simon, *Science* **2006**, *313*, 1760; d) E. Raymundo-Pinero, K. Kierzek, J. Machnikowski, F. Beguin, *Carbon* **2006**, *44*, 2498.

[4] J. S. Huang, B. G. Sumpter, V. Meunier, *Chem. Eur. J.* **2008**, *14*, 6614.

[5] J. Chmiola, G. Yushin, R. Dash, Y. Gogotsi, *J. Power Sources* **2006**, *158*, 765.

[6] A. Kajdos, A. Kvit, F. Jones, J. Jagiello, G. Yushin, *J. Am. Chem. Soc.* **2010**, *132*, 3252.

[7] C. Largeot, C. Portet, J. Chmiola, P. L. Taberna, Y. Gogotsi, P. Simon, *J. Am. Chem. Soc.* **2008**, *130*, 2730.

[8] Z. G. Cambaz, G. N. Yushin, Y. G. Gogotsi, , L. N. Pereselentseva, *J. Am. Ceram. Soc.* **2006**, *89*, 509.

[9] a) G. Yushin, A. Nikitin, Y. Gogotsi, in *Nanomaterials Handbook*, (Ed: Y. Gogotsi), CRC Press, Baton Rouge, LA**2006**, 239; b) G. Yushin, R. K. Dash, Y. Gogotsi, J. Jagiello, J. E. Fischer, *Adv. Funct. Mater.* **2006**, *16*, 2288; c) E. Lust, G. Nurk, A. Janes, M. Arulepp, P. Nigu, P. Moller, S. Kallip, V. Sammelselg, *J. Solid State Electrochem.* **2003**, *7*, 91.

[10] E. N. Hoffman, G. Yushin, T. El-Raghy, Y. Gogotsi, M. W. Barsoum, *Micropor. Mesopor. Mater.* **2008**, *112*, 526.

[11] a) E. Lust, A. Janes, M. Arulepp, *J. Solid State Chem.* **2004**, *8*, 488; b) A. Janes, L. Permann, M. Arulepp, E. Lust, *Electrochem. Commun.* **2004**, *6*, 313; c) C. Portet, G. Yushin, Y. Gogotsi, *J. Electrochem. Soc.* **2008**, *155*, A531.

[12] H. Kurig, A. Janes, E. Lust, *J. Electrochem. Soc.* **2010**, *157*, A272.

[13] P. Krawiec, E. Kockrick, L. Borchardt, D. Geiger, A. Corma, S. Kaskel, *J. Phys. Chem. C* **2009**, *113*, 7755.

[14] Y. Korenblit, M. Rose, E. Kockrick, L. Borchardt, A. Kvit, S. Kaskel, G. Yushin, *ACS Nano* **2010**, *4*, 1337.

[15] S. Shiraishi, N. Nishina, A. Oya, R. Hagiwara, *Electrochem.* **2005**, *73*, 593.

[16] R. T. Yang, *Adsorbents: Fundamentals and Applications*, Wiley & Sons, Inc., Hoboken, NJ, USA **2003**.

[17] a) P. Tan, S. Dimovski, Y. Gogotsi, *Phil. Trans. R. Soc. Lond. A* **2004**, *362*, 2289; b) A. C. Ferrari, J. Robertson, *Phil. Trans. R. Soc. Lond. A* **2004**, *362*, 2267.

[18] a) T. Nishida, Y. Tashiro, M. Yamamoto, *J. Fluorine Chem.* **2003**, *120*, 135; b) T. Sato, G. Masuda, K. Takagi, *Electrochim. Acta* **2004**, *49*, 3603; c) S. Kim, S.-J. Park, *Electrochim. Acta* **2009**, *54*, 3775.

[19] a) R. K. Dash, G. Yushin, Y. Gogotsi, *Micropor. Mesopor. Mater.* **2005**, *86*, 50; b) E. Hoffman, G. N. Yushin, B. M. Barsoum, G. Gogotsi, *Chem. Mater.* **2005**, *17*, 2317.

[20] R. De Levie, *Electrochim. Acta* **1963**, *8*, 751.

[21] J. Chmiola, G. Yushin, R. K. Dash, E. N. Hoffman, J. E. Fischer, M. W. Barsoum, Y. Gogotsi, *Electrochem. Solid State Commun.* **2005**, *8*A357.

[22] D. W. Wang, F. Li, M. Liu, G. Q. Lu, H. M. Cheng, *Angew. Chem.Int. Ed.* **2008**, *47*, 373.

[23] Y. Liang, X. Feng, L. Zhi, U. Kolb and K. Mullen, *Chem. Comm.* **2009**, 809-811.

[24] a) B. E. Conway, *Electrochemical Supercapacitors: Scientific Fundamentals and Technological Applications*, Springer, New York **1999**; b) A. G. Pandolfo, A. F. Hollenkamp, *J. Power Sources* **2006**, *157*, 11.

[25] a) C. Portet, G. Yushin, Y. Gogotsi, *Carbon* **2007**, *45*, 2511; b) K. G. Gallagher, G. Yushin, T. F. Fuller, *J. Electrochem. Soc.* **2010**, *157*, B820.

Received: October 25, 2010
Revised: December 20, 2010
Published online: March 30, 2011

